

Analysis and Design of Modular Composite Walls for Combined Thermal & Mechanical Loading

A. H. Varma^a, S. R. Malushte^b, K. C. Sener^a, and P. N. Booth^a

^a School of Civil Engineering, Purdue University, West Lafayette, IN, USA

^b Bechtel Power Corporation, Frederick, MD, USA, smalusht@bechtel.com

Keywords: Modular Composite Walls, Thermal Behavior, Temperature Gradient, Thermally-induced Moment, SC Walls, Combined Thermal and Mechanical Loading

1. ABSTRACT

This paper presents the out-of-plane flexural behavior and design guidelines for steel-plate reinforced concrete (SC) wall systems subjected to simultaneous mechanical and thermal loading. A fiber-based analytical approach was used to predict the fundamental behavior of steam generator compartment walls subjected to postulated accident causing about 10 psi uniform internal pressure and exposed surface temperature of 300°F for duration of two hours. The analytical approach was verified by using it to predict the experimental behavior of SC specimens tested previously by the authors. The analytical results were used to develop simple design guidelines for calculating stresses in the steel faceplates of SC walls subjected to simultaneous thermal and mechanical loading. Lastly, the analytical approach is used to predict and compare, i.e., illustrate similarities and differences between the behavior of SC and conventional reinforced concrete RC walls subjected to simultaneous thermal and mechanical loading.

2. INTRODUCTION

SC modular walls are experiencing increasingly widespread use in nuclear power plant construction. This technology has proven to be beneficial in applications that place a premium on accelerated construction schedule. This is largely due to the fact that SC designs lend themselves well to prefabrication and modularization while eliminating formwork and most rebar. This substantially reduces field labor costs compared to conventional reinforced concrete construction, as it involves significant field labor for formwork and rebar [1]. Prefabrication also reduces overall labor expenses by directing costs away from the field and into fabrication facilities that provide higher levels of quality, productivity, and automation. In addition, SC structural systems have demonstrated desirable structural properties such as high ductility during ultimate loading and ease of repair that make their use well suited for many applications [2].

The economic benefits of SC structural systems have generated increased interest into their applicability to a wide array of possible future uses, including those involving blast/missile resistant designs. The purpose of this paper is to develop simple design/analysis tools that are necessary to model the SC wall behavior subjected to simultaneous thermal and pressure load using an analytical approach. Literature survey indicates that there is ample test/analytical data on the behavior of SC walls subjected to mechanical loads, but not on combined thermal and mechanical load. Concrete tends to become “fully cracked” when subjected to high temperature gradient (i.e., concrete ceases to contribute in compression). Under such loading environment, it is vital that the steel plates continue to act as “bonded rebar” (i.e., not experience failure due to local buckling and/or shear connector) and that the section maintains sufficient resistance to out-of-plane shear and bending. Furthermore, the wall should be able to resist beyond-design-basis pressure loads without risking an imminent/brittle collapse mode. Finally, simple design/analysis tools are necessary to model the SC wall behavior subjected to simultaneous thermal and pressure load. With this in mind, a research project including experimental and

analytical studies was conducted to address these issues / concerns [3]. The results from the experimental investigations were outlined earlier by the authors [4]. This paper presents the fiber model analytical approach that was developed to investigate the SC wall application by comparing the analytical results with experimental data [3, 4].

3. ANALYTICAL INVESTIGATIONS OF BEHAVIOUR

The analytical investigations focused on: (a) developing of an analytical approach for predicting the thermal and structural behavior of SC specimens tested previously by the authors [3, 4], (b) verifying the analytical approach using experimental results, and (c) developing simple design guidelines for determining stresses in the steel faceplates and evaluating the effects of end fixity. The analytical approach consisted of modeling the fundamental behavior (moment-curvature-temperature relationship) of the SC cross-section using a fiber model, and numerically integrating it along the length to predict the structural behavior of the member.

The basic $M - \phi - T$ behavior was modeled and predicted using a fiber model of the SC specimen cross-section. The fiber model approach was used because experimental observations did not indicate any local buckling of the steel plates, or significant slip at the shear connector locations [3, 4]. This is important because the fiber model assumes plane sections remain plane and perpendicular to the neutral axis before and after heating and bending, which would be violated by local buckling and/or significant slip. The fiber model approach was also selected because of its ability to deal efficiently with concrete tensile cracking, which would be difficult to model effectively with the 3D finite element method.

The fiber model was implemented with a computer program that computed the complete $M - \phi - T$ response of the specimen cross-section for a specific section geometry (wall thickness, steel plate thickness, etc.), material properties (steel yield stress, concrete strength, thermal expansion coefficients, etc.), and temperature gradient (non-linear profile) through the cross section.

At any time instant (before, during, or after heating), the temperature distributions and thermal gradients through the specimen cross-section were calculated by performing thermal analysis of the fiber model. The calculated fiber temperatures were used to determine the section $M - \phi - T$ behavior for various elapsed times, since the temperature distributions and gradients are a function of elapsed/exposed time. This section response was used to estimate the curvature distributions (corresponding to the moment distribution) at discrete locations along the specimen length. Finally, the curvature distributions were integrated numerically using the moment area principle to calculate the beam deflections and distribution. The whole process was repeated for various exposure times using the corresponding calculated temperature gradients. Thus, the structural behavior of the specimen was predicted before, during, and after heating using the fiber model approach.

3.1 Mathematical Modelling

Fiber models of the composite SC cross-section were developed. The assumptions of the fiber modeling approach were as follows:

1. Plane sections remain plane and perpendicular to the neutral axis before and after heating.
2. The cross-section can be discretized into layers of material fibers or elements.
3. These fibers do not slip relative to each other and are subjected to uniaxial stress-strain only.
4. The shear deformation and strains are small.

Poh's [5] stress-strain model was used for the steel fibers at ambient and elevated temperatures. Elastic modulus $E = 29,000$ ksi and yield stress $F_y = 50$ ksi were used at ambient temperatures. At the elevated temperature of $300^\circ F_y$, the steel yield stress and the elastic modulus were both assumed to reduce according to Poh's equations. The Popovics [6] stress-strain model was used for the concrete fibers in compression at ambient and elevated temperatures.

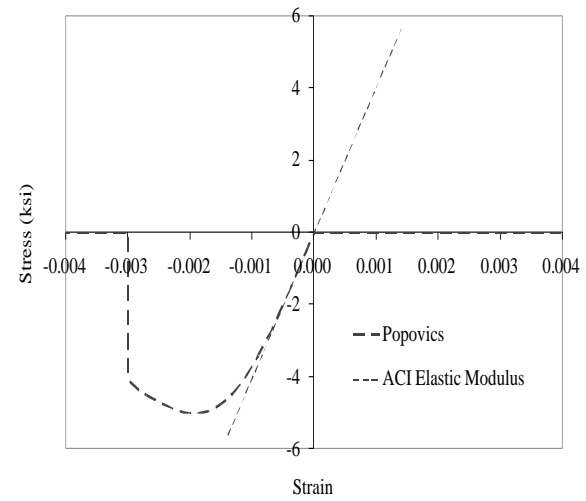
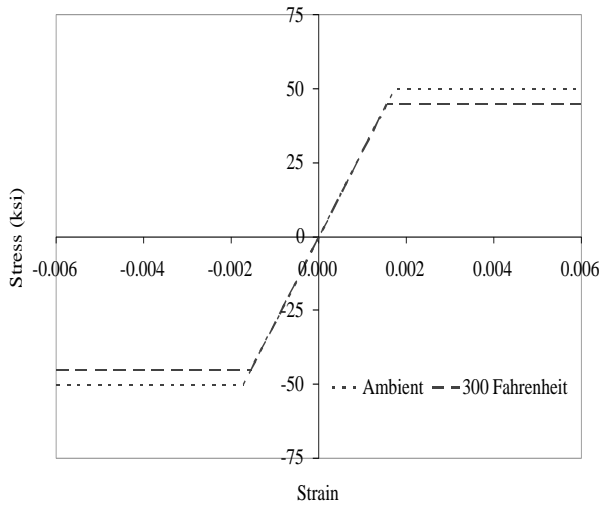


Figure 1. Fiber Model Steel Stress-Strain Curve **Figure 2.** Fiber Model Concrete Stress-Strain Curve

The concrete temperatures were always less than 300° F. The Eurocode stress-strain-temperature models do not predict significant differences in the ambient and elevated temperature stress-strain behavior of concrete at 300° F. Hence, the same (Popovics) stress-strain model was used for the ambient and concrete fibers. This stress-strain model is shown in Figure 2. As shown, it provides an approximately linear response until 50% of maximum stress followed by nonlinear softening until peak compressive stress (5,000 psi). The concrete strain at compressive failure was set to 0.003. Additionally, the concrete was assumed to have zero tensile strength. The initial stiffness was calculated using the ACI equation for elastic modulus (E_c) based on compressive cylinder strength (f'_c).

The composite SC cross-section was discretized into a total of 4 steel fibers and 30 concrete fibers. The thermal loading was applied by heating one side (i.e., the top faceplate) of the beam specimen to 300° F in the initial 10 minutes, and sustaining this temperature for 2 hours. Figure 3(a) shows the temperatures and thermal gradients obtained from the thermal analysis. It includes the temperature distribution after 15 minutes, 45 minutes, and 120 minutes of heating. Figure 3(b) shows the corresponding experimentally measured temperatures and thermal gradients [3, 4]. Figures 3(a) and (b) show that the: (i) thermal gradients have significant nonlinearity, (ii) concrete temperatures within the section depth increase gradually with time as heating is maintained, and (iii) the analytical approach predicts the experimental temperatures and thermal gradients with reasonable accuracy.

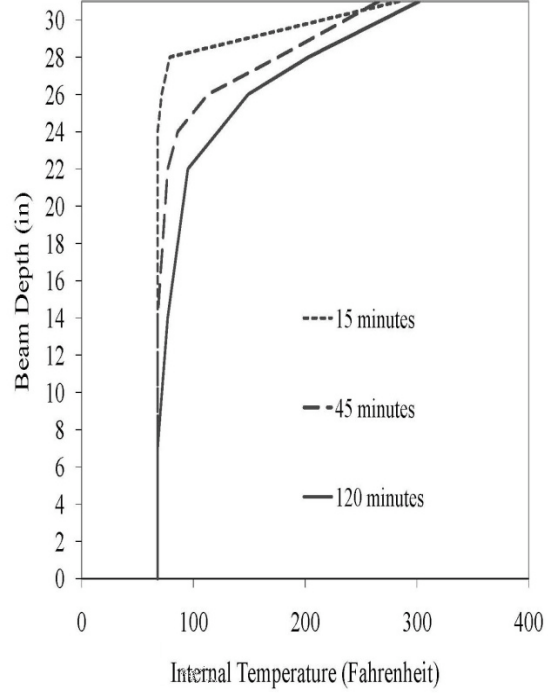
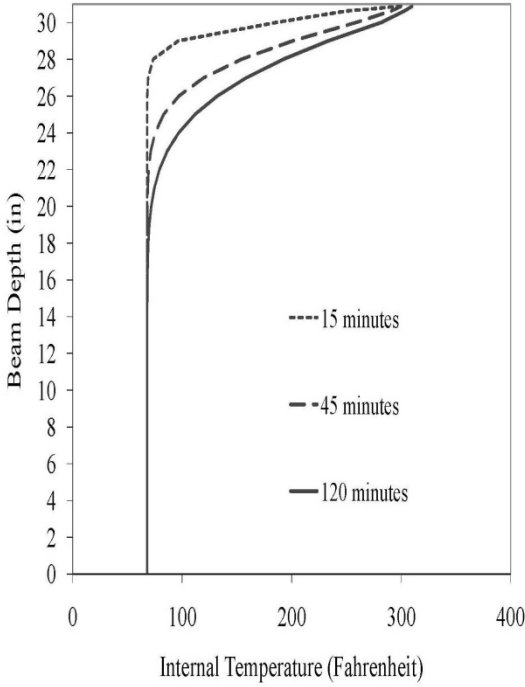


Figure 3a. Analytically Determined Thermal Gradient **Figure 3b.** Experimentally Determined Thermal Gradient

The thermal strain (ϵ_{th}) for each fiber was calculated as the material thermal expansion coefficient (α) multiplied by the temperature increase (ΔT_{fib}). The material thermal coefficients for steel (α_s) and concrete (α_c) were assumed to be equal to $6.5 \cdot 10^{-6} / ^\circ F$ and $5.5 \cdot 10^{-6} / ^\circ F$, respectively. These values were based on the AISC Specification (AISC 360-05). The coefficients were assumed to remain constant within the temperature range of ambient to $300^\circ F$.

3.2 Fiber Model Methodology

Figure 4 shows the complete flowchart for calculating the section moment-curvature ($M - \phi$) response at any time instant. As shown, the section is divided into several steel and concrete fibers. Each fiber is associated with area (A_{fib}), distance from centroid (y_{fib}), and material stress-strain (steel or concrete). The cross-section temperature distribution at the time instant was used to assign the temperature (T_{fib}) to all fibers of the cross-section. The fiber temperatures were used to calculate the thermal strain (ϵ_{th-fib}) using Equation (1) shown below:

$$\epsilon_{th-fib} = \alpha_m \cdot \Delta T_{fib} \quad (1)$$

where: α_m equals to α_s or α_c depending on the material
 ΔT_{fib} = Change in the fiber temperature from ambient

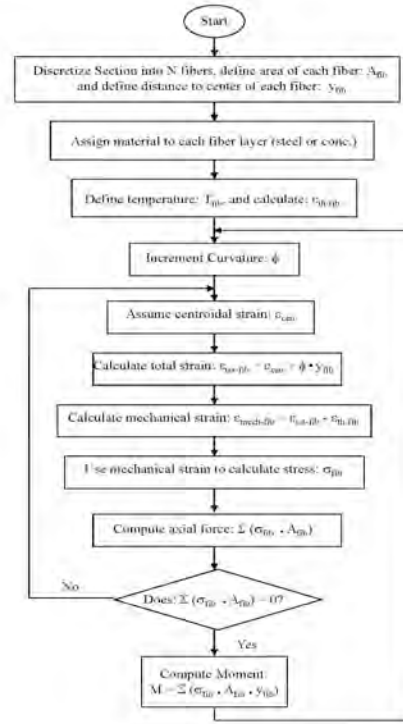


Figure 4. Fiber Model Flow Chart for Calculating Moment-Curvature Response

The section curvature (ϕ) is assumed to begin with, and iterations are performed to find section equilibrium as follows. The centroidal strain (ϵ_{cen}) is assumed for the current curvature (ϕ). The total strain in each fiber ($\epsilon_{tot-fib}$) was calculated using Equation (2). The mechanical strain in the fibers was calculated using Equation (3).

$$\epsilon_{tot-fib} = \epsilon_{cen} + \phi \cdot y_{fib} \quad (2)$$

$$\epsilon_{mech-fib} = \epsilon_{tot-fib} - \epsilon_{th-fib} \quad (3)$$

The fiber mechanical strains ($\epsilon_{mech-fib}$) were used to determine the stresses (σ_{fib}) resisted/carried by them from the appropriate material (steel ambient temperature, steel elevated temperature, or concrete) - curves. The fiber stresses (σ_{fib}) were multiplied by the corresponding areas (A_{fib}) and summed over the section to calculate the section axial force. If the section axial force is not equal to the applied force (zero), then the centroidal strain (ϵ_{cen}) assumption is improved. Iterations are performed to determine the centroidal strain (ϵ_{cen}) corresponding to the curvature (ϕ), that provides section equilibrium. After section equilibrium is obtained, the section moment corresponding to the equilibrium state and the selected curvature value (ϕ) are calculated using Equation (4):

$$M = \sum \sigma_{fib} \cdot A_{fib} \cdot y_{fib} \quad (4)$$

The curvature is the incremented to a new value, and the whole process is repeated to find the corresponding moment (M). The pairs of moment and curvature data are used to construct the section M - ϕ at the time instant with given thermal distributions.

4. RESULTS AND DISCUSSION

Figure 5 presents the section moment-curvature ($M - \phi$) responses predicted for the specimen having concrete thickness of 30 inches and steel faceplate thickness of 0.5 inches. Figure 5 includes the $M - \phi$ responses for three conditions: (1) ambient with no thermal gradient; (2) after 15 minutes of heating with temperature distribution shown in Figure 3a and (3) after 120 minutes of heating with temperature distribution shown in Figure 3a.

Figure 5 shows that the initial thermal gradient (after 15 minutes of heating) causes the $M - \phi$ diagram to shift to the left with non-zero curvature at zero moment, and non-zero moment for zero curvature. This shift is produced by the thermal gradient in the section. The curvature corresponding to zero moment is referred to as thermal curvature (ϕ_{th}). The moment corresponding to zero curvature is referred to as the thermal moment (M_{th}). Figure 5 also shows that the $M - \phi$ response of the specimen subjected to final thermal gradient (after 120 minutes of heating) is also shifted to the left with non-zero curvatures at zero moments. The $M - \phi$ response for the final thermal gradient (after 120 minutes) is very similar to that for the initial gradient (after 15 minutes). In particular, the thermal curvature (ϕ_{th}) and moments (M_{th}) are almost identical for the two different thermal gradients.

The $M - \phi$ response for the final thermal gradient shows that the tangent stiffness eventually increases with increasing moments until the peak moment is reached. The increase at higher applied moments is also more pronounced for the final temperature gradient compared to the initial gradient. This is due to concrete expansion at the top of the section which tends to close cracks and reengage concrete in compression above the neutral axis. The calculated moment capacities for the cases with thermal gradients are slightly higher than the ambient moment capacity. This occurs due to the variations in the depth of engaged concrete in the section at the ultimate stage due to the thermal gradient profile.

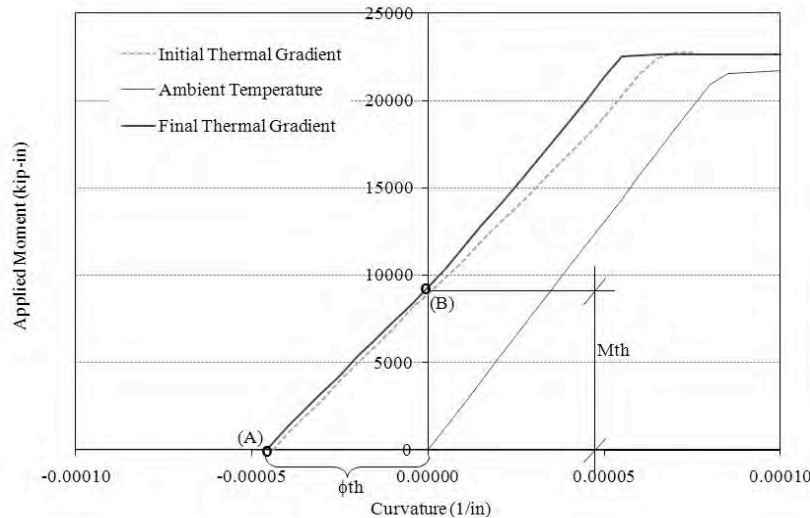


Figure 5. Fiber-Model Moment Curvature Plots

Figure 5 includes markers (A) and (B) to indicate the occurrence of thermal curvature (ϕ_{th}) and thermal moment (M_{th}). The complete curvature, strain, and stress distributions corresponding to these locations (A) and (B) are tabulated in Figures 6 and 7, respectively for the SC specimen with 0.5 in. faceplate thickness. These figures include: (i) the curvature distribution (ii) thermal gradient, (iii) thermal strains, (iv) mechanical strains, (v) steel stresses, and (vi) concrete stresses for each of these locations (A) and (B) on the $M - \phi$ response. These results were determined directly from the fiber analysis of the SC cross-section.

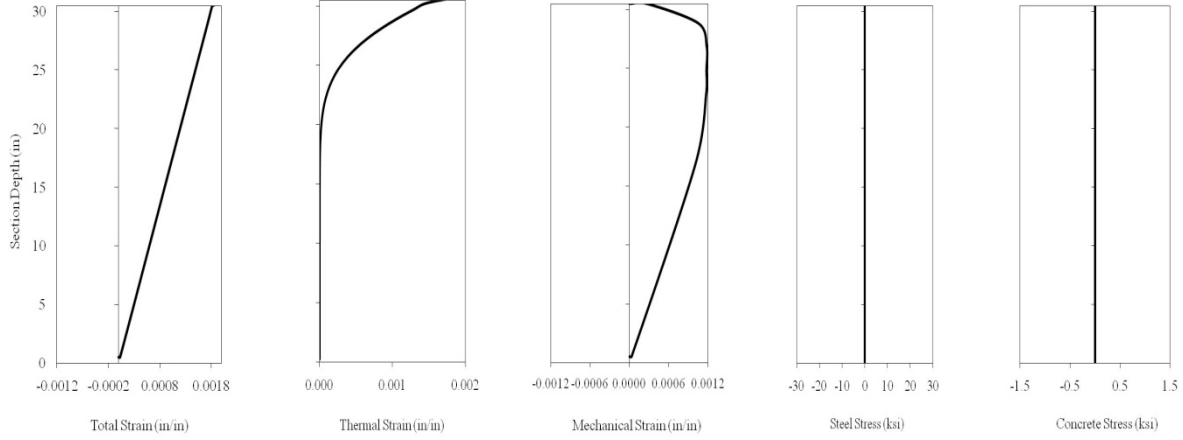


Figure 6. Strains and Stresses at ϕ_{th} i.e., location A on $M-\phi$ response of SC section with 0.5 in. thick faceplates

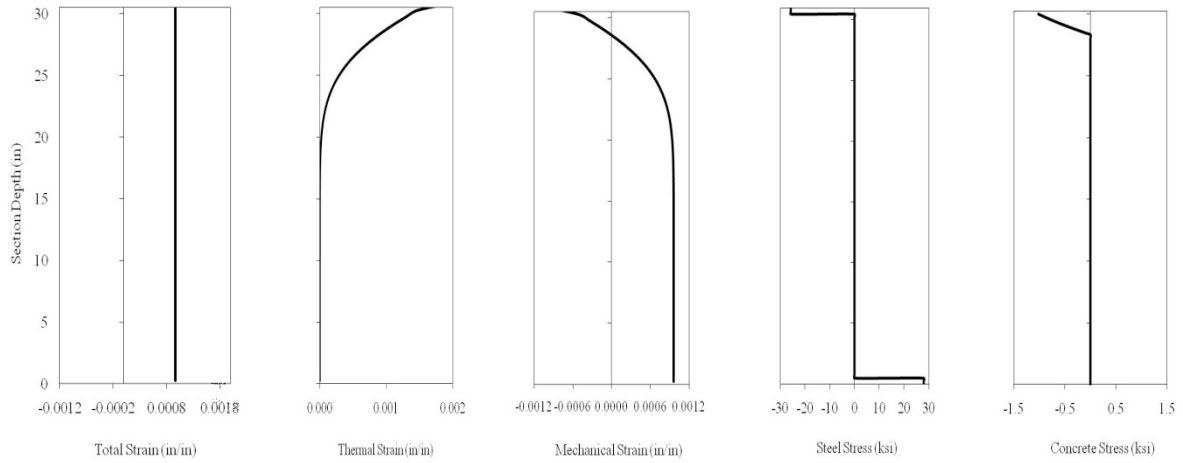


Figure 7. Strains and Stresses at M_{th} i.e., location B on $M-\phi$ response of SC section with 0.5 in. thick faceplates

The results from the fiber analysis shown in Figure 6 indicate that for location A, which corresponds to the specimen subjected to thermal gradient and zero moment, the mechanical strains in the concrete ($\epsilon_{tot} - \epsilon_{th}$) are tensile through the entire section. Thus, the thermal gradient cracks the entire concrete section. The axial force and moment in the composite section are zero. As a result, force equilibrium is only possible with the neutral axis in the bottom steel plate, and the top steel plate subjected to mechanical strain equal to zero (see Figure 6 obtained from fiber model results). This means that the total strain in the top steel plate is equal to the thermal strain (ϵ_{th}). As a result, the thermal curvature (ϕ_{th}) will be equal to $\frac{\alpha_s \cdot \Delta T_s}{d - t_s}$ as shown in Equation 5:

$$\phi_{th} = \frac{\epsilon_{tot-top}}{d - t_s} = \frac{\epsilon_{th-top}}{d - t_s} = \frac{\alpha_s \cdot \Delta T_s}{d - t_s} \quad (5)$$

where:

$\epsilon_{tot-top}$ = total strain in steel top plate

ϵ_{th-top} = thermal strain in steel top plate

$$\Delta T_s = \text{temperature change in top plate}$$

4.1 Deflection Verification

Beam deflections were calculated using the moment area theorem in conjunction with the fiber model section moment curvature output. The model SC wall span had pinned boundary conditions at wall intersections and the wall length was assumed equal to 22 ft, the wall thickness was 30 inches, and the steel plate thickness equals 1/2 inches. Figure 8 presents deflections calculated for SC Specimen 1 tested previously by the authors [3, 4]. The Figure compares the analytically predicted and experimentally measured deflections for all three loading phases during the test, i.e.: (i) the initial ambient loading of 25 kips, which corresponds to 10 psi uniform internal pressure, (ii) heating of the top plate for 2 hours while maintaining the loading at 25 kips, and (iii) increasing the applied loading to 90 kips, which corresponds to 36 psi uniform internal pressure, after two hours of heating.

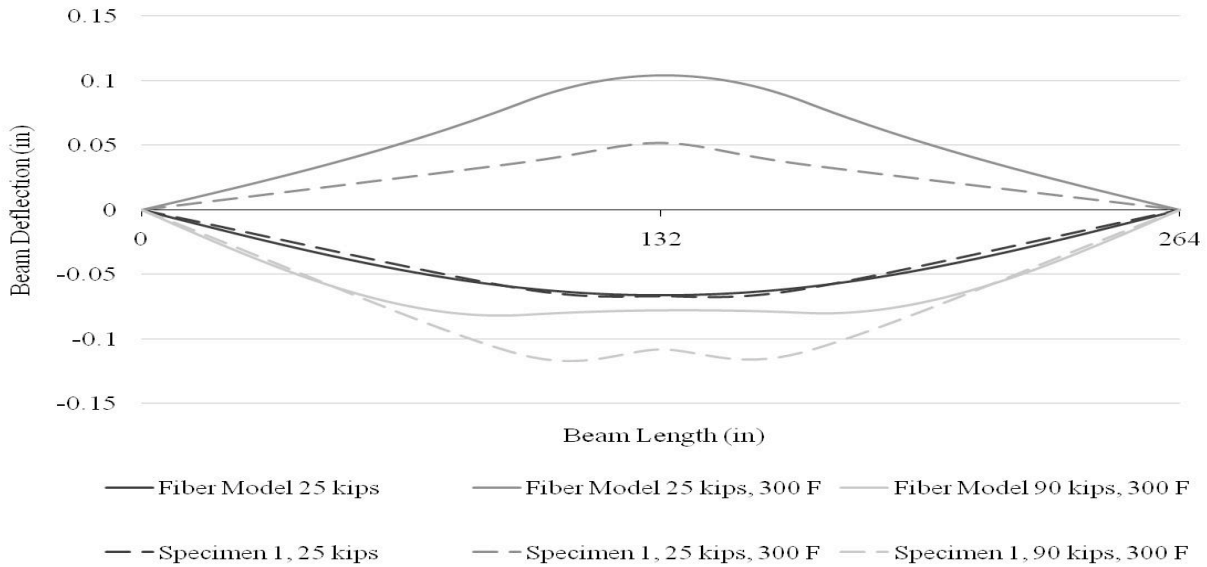


Figure 8. Deflected Shape Comparison for Fiber Model and the Specimen

The Figure shows that the fiber model approach slightly overpredicts the specimen deflections during the heating and final loading phases. The over prediction of thermal deformation can be attributed to a number of factors, namely, non-uniform heating of the steel top plate, resistance of concrete in tension (which is ignored in fiber model), and small slippage between the steel plates and concrete. The discrepancies in deflection prediction were also partly due to non-uniform heating in the beam midspan region. The area at the center of the beam was believed to be slightly hotter than at load points due to heat loss at the edges of the heaters. Also, the exposed concrete sidewalls provided a free surface for heat flux losses that were not taken into account in the section model.

Over prediction of deflections also resulted from the fact that the fiber model did not account for partial composite action and contribution of concrete in tension. Partial composite behavior was demonstrated during the tests via slip measurements taken between the upper steel plate and underlying concrete interface. Slip along this plane would tend to reduce concrete tensile stresses during differential expansion of the upper plate thus reducing the stress gradient in the concrete section and corresponding curvature. Slip was omitted from the model since little was known about its interaction with thermal effects. Conversely, concrete tensile stress would work to restrain the upper steel plate during thermal expansion also reducing deflections.

4.2 Fiber Model Verification

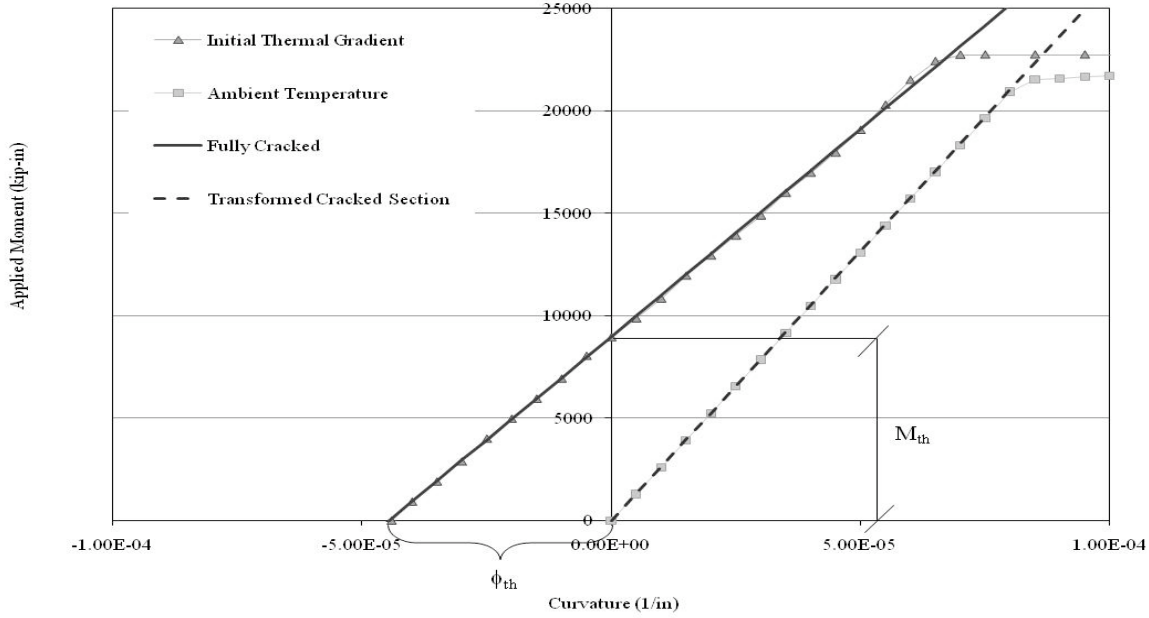


Figure 9. Comparison of Fiber Model Moment Curvature to Transformed Cracked and Fully Cracked Moment of Inertia

Figure 9 shows comparisons of the fiber model $M-\phi$ curves with flexural rigidity (EI) values based on cracked-transformed section and fully cracked section properties. The $M-\phi$ behavior before heating followed the cracked-transformed section stiffness, which is consistent with conventional reinforced concrete section behavior. After heating, the differential expansion between steel and concrete resulted in complete concrete cracking in the model (see Figure 6 and 7) and the section $M-\phi$ behavior followed the fully cracked section stiffness, i.e., the stiffness provided by the steel plate alone. As shown in Figure 9, the thermal moment (M_{th}) can be related to the thermal curvature (ϕ_{th}) using the fully cracked section stiffness. This relationship is given by Equation 6. As mentioned earlier, the thermal curvature (ϕ_{th}) can be related to the temperature increase (T) in the top surface plate using Equation 5. Combining Equations (5) and (6), the thermal moment (M_{th}) can be calculated easily using Equation 7.

$$M_{th} = \phi_{th} \times EI_{cracked} \quad (6)$$

$$M_{th} = \frac{\alpha_s \cdot \Delta T_s}{d - t_s} \times EI_{cracked} \quad (7)$$

4.3 Comparison with Conventional RC Section

Figures 10 and 11 present and compare the $M - \phi$ responses of the SC and RC systems, respectively. In this comparison, the overall section dimensions were kept the same by using 30 inches depth and 12 inches width, i.e., 1 foot unit width. Steel ratio in the sections were also kept at the same value by using 0.26 in steel faceplate in the SC section and using #11 rebars at 6 inches spacing as reinforcement steel in the RC section. Location of reinforcement steel is a crucial parameter in the response of the RC section. Therefore 2 in. of clear cover was assumed because it is commonly used in design and the field.

As shown in Figure 10, thermal curvature (ϕ_{th}) and thermal moments (M_{th}) in the SC system are very much similar at increased thermal gradients as previously stated for the 0.50 inch steel faceplate case. However, as shown in Figure 11 for the RC system, these parameters vary significantly with the change in the thermal gradient. As expected, the thermally induced moment at zero curvature is smaller for RC sections because, unlike the SC section, the rebar in RC section is insulated from direct thermal exposure by the presence of the concrete cover. This reduces the temperature increase experienced by the rebar on the hot side and in turn reduces the moment induced into the RC cross-section.

As seen from Figures 10 and 11, there is one-third reduction in the M_{th} moment for an RC section compared to an SC section of an equal reinforcement. While this appears dramatic, the SC sections typically involve higher rebar ratio to help resist the construction loads and to meet the local buckling criteria such that the portion of their capacity used up by M_{th} does not pose any challenge in terms of their reserve capacity. For example, Ref. [3] has demonstrated that SC sections can resist mechanical loads well in excess of three times their design loads while being subjected to the design temperature loading.

Similar to the M_{th} equation presented herein for the SC system, the authors are continuing to work on developing an empirical equation for the thermally induced moment for a given exposure time and exterior temperature for an RC system.

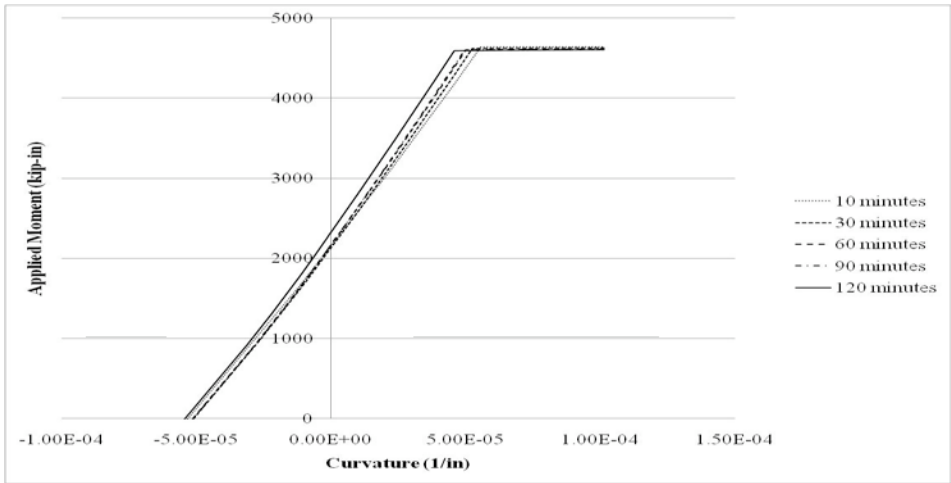


Figure 10. Moment-Curvature Response of SC system having 0.26 in. thick faceplate

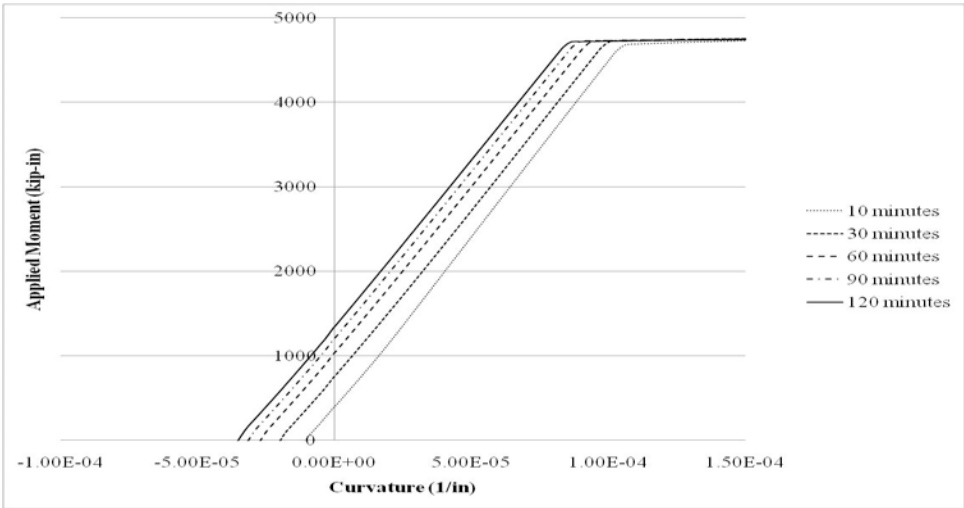


Figure 11. Moment-Curvature Response of RC system having #11 bars at 6 in.

5. CONCLUSIONS

This paper presented the development and verification of a fiber model approach for predicting the behavior of composite SC section subjected to simultaneous or combined thermal and mechanical loading from an accident scenario. The analytical results indicated that:

- 1) Thermal loading produces a highly nonlinear temperature gradient in the composite cross-section.
- 2) The thermal gradient shifts the section moment-curvature response such that there is a non-zero thermal curvature (ϕ_{th}) corresponding to zero moment, and a non-zero thermal moment (M_{th}) corresponding to zero curvature.
- 3) ϕ_{th} corresponds to the behavior of a beam with pin ends, i.e., free to rotate. M_{th} corresponds to the behavior of a beam with fix ends, i.e., restrained against rotation ($\phi=0$).
- 4) 4) The thermal gradient results in concrete cracking through the depth of the section, and the flexural stiffness is reduced to that of a fully cracked section.
- 5) A simple design equation can be used to estimate both ϕ_{th} and M_{th} using the fully cracked section stiffness, section depth, thermal expansion coefficient of steel, and the temperature increase of the exposed faceplate.
- 6) The analytical approach presented here can also be used to predict the behavior of RC sections subjected to combined thermal and mechanical loading. The behavior of RC sections is similar, but somewhat different from that of SC sections.

***Acknowledgments:** This research was funded by Bechtel Corporation and Purdue University. Special thanks are due to Mr. Anil Agarwal and Dr. Victor Hong for their assistance with the analytical work.*

REFERENCES

1. MPR-2610 Revision 2, "Application of Advanced Construction Technologies to New Nuclear Power Plants", Department of Energy Report, September 2004, <http://www.ne.doe.gov/np2010/reports/mpr2610Rev2Final924.pdf>
2. Adams, P. F., Zimmerman, T. J. E., "Design and Behaviour of Composite Ice-Resisting Walls", "Steel/Concrete Composite Structural Systems," C-FER Publication No. 1, Proceedings of a Special Symposium held in Conjunction with POAC '87, Fairbanks, Alaska, 9th International Conference on Port and Ocean Engineering under Arctic Conditions, 1987.
3. Booth, P.N. "Behavior of Steel Plate Reinforced Concrete Modular Walls Subjected to Combined Thermal and Mechanical Loads." M.S. Thesis, Purdue University, School of Civil Eng., West Lafayette, IN 47906
4. Booth, P.N., Varma, A. H., Malushte, S. R., Johnson, W. H., "Response of Modular Composite Walls to Combined Thermal & Mechanical Load", SMiRT-19, IASMiRT, Toronto, Canada, August 2007, 10 pp.
5. Poh, K. W., "Stress-Strain-Temperature Relationship for Structural Steel", Journal of Materials in Civil Engineering, ASCE, Vol. 13, No. 5, September/October, 2001, pp. 371-379.
6. Popovics, S., Mechanical Behavior of Materials, Proceedings of the International Conference on Mechanical Behavior of Materials, Vol. IV., The Society of Materials Science, Japan, 1972, pp. 172 – 183.